

Inverting the Relationship of Fuel and Coolant

W. Van Snyder*

^aIndependent Researcher

*Email: van.snyder@sbcglobal.net

Number of pages: 29

Number of tables: 15

Number of figures: 6

Abstract

In EBR-II, fuel was contained within fuel pins and surrounded by coolant. That relationship could be inverted in a future LMFBR: Motile fuel, composed of fine metallic particles mixed with sodium for thermal bond, contained within a hexagonal unit cell penetrated by coolant tubes. An exhaust port connected to a plenum above the fuel within the unit cell would remove fission-product gases, especially the powerful neutron poison xenon, and maintain pressure within the unit cell in the range of the pressures in the coolant tubes or surrounding environment, thereby eliminating radial strain due to fission gas pressure. Fuel/container mechanical interaction would be reduced or eliminated. Fuel element durability, and therefore burnup, would be increased. Fuel volume fraction would be increased, which would improve neutron economy, increase breeding ratio, reduce initial fuel load fissile enrichment, reduce reactivity swings during burnup, and allow a smaller reactor for the same power output. Stored doppler reactivity is reduced because thermal conductivity of sodium-plus-uranium paste is greater than that of uranium alone at all operating temperatures. This monograph describes only a thermal-hydraulic analysis of a single unit cell in this configuration. Neutronic, criticality, control, stability, and safety analyses, and more complete thermal-hydraulic and structural analyses of a complete reactor, are outwith the scope of this study.

Keywords — metallic fuel, finely divided fuel, coolant within fuel

I. INTRODUCTION

In [1, pp. 308-309], Till and Chang remarked “to maintain a hard spectrum, the fuel volume fraction needs to be maximized in the core lattice design. . . . [H]igher fuel volume fraction design gives better neutron economy, resulting in lower fissile enrichment, a higher internal conversion ratio, and a reduced reactivity swing during burnup.” It also allows a smaller reactor for the same power output.

In contemporary reactors, fuel is contained within pins and surrounded by coolant. Figure 1 illustrates a proposal to invert that relationship: Contain fuel within a hexagonal unit cell, with coolant tubes passing through fuel, and surrounded by coolant. Choose the 2τ spacing between unit cells such that the velocities of coolant flowing around the unit cell and through the coolant tubes, and therefore the pressure gradients in those regions, are the same.

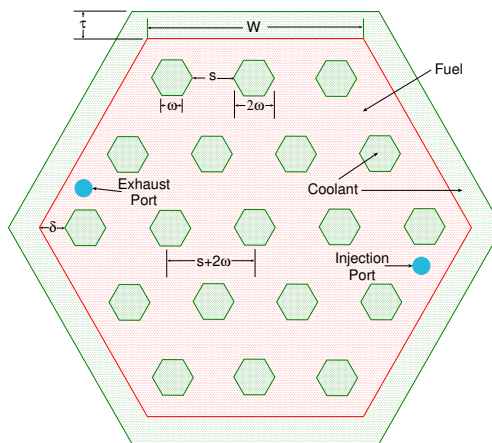


Fig. 1. Unit cell

Inverting the relationship allows a higher fuel volume fraction, with the attendant benefits described above. Unlike the case with numerous fuel pins within an assembly, it is feasible to connect an exhaust port to a plenum above the fuel, to remove fission-product gases, especially the powerful neutron poison xenon, and to maintain pressure within a unit cell in the range of the pressures in the coolant tubes or surrounding environment.^a

According to [1, p. 116], [2], and [3, p. 2], the primary limitation to fuel burnup in the Experimental Breeder Reactor II (EBR-II) was fuel pin cladding durability, and bundle-duct interaction due to radial fuel pin strain. Radial strain from fission product gas pressure is eliminated in this concept by controlling the pressure within the unit cell. Reducing internal gas pressure can compensate for and reduce the effect of radial strain due to the weight of fuel.

^aAlthough xenon would have a smaller effect on neutron economy in LMFBR because of its smaller absorption cross section for fast neutrons than for thermal neutrons, it produces 90% of fission product gas pressure.

II. FUEL COMPOSITION

One way to invert the relationship between fuel and coolant is to fabricate solid fuel slugs, somewhat smaller than a unit cell, with holes somewhat larger than coolant tubes, and use sodium for thermal bond. This might be possible by vacuum or injection casting. Drilling holes after casting would be undesirable. Alternatives include cast “zigzag” blocks that would fit around coolant tubes, or thin sheets in which holes are punched.

During burnup, solid metallic fuel would expand, in bulk outward toward the edge of the unit cell, and inward toward coolant tubes, partly due to lower density of fission products, but primarily due to accumulation of sealed pores of fission gases [4] [2, p. 90]. This might rupture the outer wall of the unit cell, or crush coolant tubes. To cope with that, lower initial fuel volume density, or more robust structure, would be necessary, both of which would decrease the fuel volume fraction and lead to reactivity swings during burnup. Fuel slugs in EBR-II were fabricated with diameters about 85% of the inner diameter of cladding [1, p. 123].

To avoid those problems, fabricate fuel as a paste of small particles of polydisperse sizes mixed with sodium for thermal bond. This is only feasible in a sodium-cooled reactor. For a water-cooled reactor, it might be possible to use zinc for thermal bond. The volume mixing ratio of fuel within the paste would be in the range 65%-95%, depending upon particle size distribution [5], and the relationship of fuel particle sizes to container size and shape. Smaller average particle size reduces container boundary effects on fuel density, and increases fission product transfer to bond sodium.

An alternative to a fuel/sodium paste is molten salt, but this exacerbates fuel/container chemical interaction (FCCI).

With motile fuel, bulk expansion due to burnup would all be in the axial direction, and much less than with solid fuel because fission gases would largely escape from particles instead of forming sealed pores. With a plenum above fuel, to accommodate fuel expansion and fission-product gases, and with the plenum connected to an exhaust port, fuel would not put stress on the container, other than by its weight.

A more complete discussion of particulate fuel in sodium appears in [6].

Stringent limits are placed on power variations in oxide reactors due to stresses on fuel. This is one of the reasons that conventional nuclear power reactors are not used for load following. Solid

metallic fuel in EBR-II was significantly less affected by power variations [1, p. 130]. A sodium paste fuel would be even less affected.

III. STRUCTURE OF A UNIT FUEL CELL

The unit cell is constructed from HT-9 (Martensitic) stainless steel.

A solid HT-9 billet is hot-extruded into a heavy-walled circular cylinder.

The circular tube is passed through an induction heating coil that brings the metal to its plastic state ($\approx 1,100^\circ\text{K}$) without melting it.

The heated duct is pulled through a series of tungsten-carbide hexagonal dies while a matching internal mandrel travels inside the tube.

This “squeezes” the circular tube into the precise desired flat-to-flat hexagonal profile and ensures a perfectly uniform wall thickness.

A final “skin-pass” is performed at room temperature to achieve the mirror-finish and the final dimensional tolerance required.

Heat to $1,310^\circ\text{K}$ to dissolve carbides and transform the grain structure into austenite.

Air quench to rapidly transform the austenite into fresh, untempered martensite.

Re-heat to $1,030^\circ\text{K}$ to “toughen” the martensite. This stabilizes the carbides at the grain boundaries, which is the specific mechanism that prevents void swelling

Coolant tubes are stabilized against bending and vibration by two equally-spaced horizontal HT-9 “spider web” structures that are welded to the corner spines, and maybe to the central tube. The spider webs have a 30° sloping boss around each tube so as not to form a “dead corner” where fuel could stagnate. It is not necessary to weld them to other tubes. A 0.2 mm radial slip fit is tight enough to prevent “fretting wear” during vibration but loose enough to allow for differential thermal expansion.

Coolant tubes need not be circular. If they are hexagonal, arranged on a triangular lattice, the average distance from a fuel particle to the surface of a coolant tube is more uniform than with circular tubes. By choice of size and placement, spacing between edges of coolant tubes can be made uniform, thereby making the average distance between fuel particles and coolant more uniform throughout the unit cell, or intentionally nonuniform, to account for heating differences in different regions of the unit cell — but as will be seen in Table II, although temperatures vary

within each region, temperatures are remarkably uniform in different regions with uniformly spaced tubes. For a particular cross-section area, a hexagonal tube has larger surface area than a circular one. This increases heat transfer from fuel to coolant, and increases structure fraction, for the same volume of coolant.

Coolant tubes are produced and attached by a more complicated process.

Hexagonal coolant tubes are manufactured using a high-precision Multi-Stage Cold Drawing (or Cold Pilgering) process. Because the tubes are made of HT-9 Ferritic-Martensitic Steel and must have a wall thickness of exactly 0.5 mm with a 3.124 mm internal width, traditional welding or extrusion is insufficient to meet the required 40-year irradiation resistance and dimensional tolerances.

The transformation from bulk steel to hexagonal reactor-grade tubing follows these steps:

A solid HT-9 billet is hot-extruded into a circular “mother tube” with a much larger diameter and wall thickness.

The circular tube is fed through a series of reciprocating rollers that reduce its diameter and wall thickness. This refines the grain structure of the HT-9, improving its strength and creep resistance.

The final shaping occurs by pulling the circular tube through a hexagonal tungsten-carbide die over a matching hexagonal internal mandrel.

This “Ironing” process creates the flats with sharp corners and uniform walls.

The cold-worked tubes are heat-treated to restore the tempered martensite microstructure, which is the key to HT-9’s legendary resistance to void swelling

The top and bottom are fabricated with 3 mm integrated interior rounded bosses that act as collars. Included collars

- spread the load of the hydraulic seating force, which prevents fatigue cracking,
- provide weld-zone isothermalization, which reduces the heat-affected zone and subsequently reduces the risk of irradiation-induced embrittlement,
- serve as “assembly jigs” that hold tubes precisely in place during final welding, and
- provide a “stiffener” at the base of each tube that preserves the natural frequency of the element and prevents “tube flutter” in the primary coolant flow.

The top and floor are formed by pressing or hydroforming.

Coolant tube holes are cut from the formed floor by lasers.

Top and bottom tubes are laser welded separately. To prevent warping due to thermal imbalance, the center tube is welded first, followed by others in an outward alternating spiral, one ring at a time, welding one tube in a 60° sector, then jumping 180° to an opposing sector. As each pair of opposing sectors is finished the process rotates 60° . The entire lattice is tack welded first, then full-penetration welds are performed in the same sequence. A rounded boss around each coolant tube, formed in the top and bottom places by the initial pressing or hydroforming before cutting the holes, reduces thermal distortions from welding.

Laser cutting and welding avoid creep, misalignment, microcracks, and radial stress.

After the coolant tubes are welded the entire assembly is again heated in a vertical furnace to below the transformation temperature to relax micro-stress zones created by welding. This eliminates weld shrinkage in-core during the first few months of 800°K operation, which might otherwise cause coolant tubes to “banana” or bow.

As described in Section IV below, coolant tubes are arranged on a regular triangular lattice. It is probably desirable to replace the six tubes nearest the corners with tubes that are integrated into the corners to stiffen the duct. Thermal and hydraulic properties of that configuration were not analyzed.

Fill the container using a low-viscosity fuel slurry; remove excess sodium as fuel settles.

It is not practical to connect the plenums of a large number of small pins to exhaust ports. It is undesirable because those connections would interfere with coolant flow. Fission-product gas pressure was a significant contributor to radial strain and to cladding damage caused by fuel/container mechanical interaction (FCMI) in EBR-II [2, p. 96], and therefore a factor limiting burnup.

With fuel contained in a unit cell, penetrated by coolant tubes, it is easy to connect the plenum using an exhaust port. Larger unit cells than in EBR-II would result in fewer connections.

Injection and exhaust ports allow the pressure inside the fuel container to be adjusted. When internal and external pressure are the same, there is no mechanical stress on the container, other than the weight of the fuel. There would be essentially no additional FCMI. The primary concerns in the design and materials of the container would be thermal-cycling stress, radiation damage,

thermal creep, and fuel/container chemical interaction (FCCI). With FCMI and structure fraction reduced, a coating or other design changes to reduce FCCI, such as the cladding barrier proposed as an option for GE S-PRISM, should be feasible [7].

Exhaust ports also remove xenon, an important neutron poison, thereby increasing burnup and further improving the ability to maintain a hard neutron spectrum.

During operation, circulate small volumes of sodium and an inert gas continuously using an injection port that extends to the bottom and an exhaust port at the top. Circulating sodium removes sodium-soluble fission products such as barium, cadmium, caesium, strontium, tellurium, . . . continuously, which would in turn allow longer burnup before fuel cycling becomes necessary. Circulating an inert gas removes xenon. Removing xenon during shutdown eliminates the “iodine pit” startup instability.

Because sodium and inert gas circulation rates are small, port tubes can be small.

Rather than connecting each port externally using a long, thin, fragile tube, connect ports of adjacent unit cells using U-shaped tubes and self-closing fittings, eventually leading to an external connection outside the core, or through a control-rod assembly. Unlike the case with numerous fuel pins within a fuel assembly, this would have a minimal effect on coolant flow.

With internal pressure slightly less than external pressure, it should be possible to attach the coolant tubes and the top of the assembly by crimping instead of welding. Alternatively, thread the ends of the tubes, with opposite pitch direction, and screw the tubes, top, and bottom together after filling, followed by crimping or welding to the sides.

Rather than replacing unit cells, refueling can be done by pumping fuel from them using an eductor powered by sodium to produce a dilute slurry, either periodically, or continuously as explained in [8].

Because there is essentially no internal mechanical stress, and in particular no shear stress because fuel is motile, there is likely no need for internal structural members or wire wrap to maintain separation between coolant tubes. This decreases structure fraction and increases fuel fraction. If coolant tubes bow due to temperature gradients, thin mid-level “spider web” structures could be incorporated. This would have minimal effect on fuel volume fraction. Unlike the case with fuel pins surrounded by flowing coolant, these would not impede coolant flow or introduce turbulence.

Design and analysis of coolant nozzles, and structural support and mechanisms to remove and replace fuel assemblies, are outwith the scope of this study.

IV. DESIGN TRADEOFFS

For a single unit cell:

- Fuel volume fraction determines power density.^b
- Power density and temperature gradient along coolant tubes determine heat removal requirements.
- Coolant fraction, heat capacity, power density, and temperature gradient determine coolant flow velocity. These are related by the hydrodynamic heat balance equation [1, §14.4.2]

$$PALf_f = 2\rho ALf_c v C_p \Delta T \text{ or } v = \frac{f_f}{2f_c} \frac{P}{\rho C_p \Delta T}, \quad (1)$$

where P is fuel power density (kW/m³), A is the cross-section area of the unit cell, excluding the surrounding coolant-flow region of thickness τ , L is the length of the reaction region of the unit cell (excluding the plenum and axial breeding blankets), f_f is fuel volume fraction, ALf_f is fuel volume, ρ is coolant density (kg/m³), f_c is coolant fraction within the unit cell, v is coolant flow velocity (m/s), C_p is coolant heat capacity (kJ/kg/°K), and ΔT is temperature gradient (°K/m) along the length L of coolant tubes. $\rho Af_c v$ is coolant flow rate (kg/s) and $L\Delta T$ is total temperature increase. The factor of 2 accounts for flow in the outer jacket region which, as will be seen below, is designed to have the same area as the total of coolant tubes' areas.

- Number and size of coolant tubes, and spacing between them within a fuel assembly, determines horizontal temperature gradients.
- Coolant flow velocity determines the pressure relationship between fuel and coolant.

^bThe number of fissions per second, and therefor the power, is given by $N(t)\sigma_f\bar{v}n(t)$, where $N(t)$ and σ_f are the number density and fission cross section of fissionable atoms, \bar{v} is the average velocity of neutrons, and $n(t)$ is the number of neutrons [9, Sec. 5.2].

The unit fuel cell is a hexagonal cell that contains hexagonal coolant tubes on a uniform triangular lattice. The corner-to-corner spacing of coolant tubes is s , and the spacing from the corner of the outermost coolant tube to the unit cell wall is δ (see Figure 1).

Referring to Figure 1, given the unit cell edge width W , thickness t_t of coolant tube walls, the number n of coolant tubes along one edge of the unit cell, the desired fuel volume fraction f_f , the volume mixing ratio ϕ of fuel within paste, and requiring the cross-section area of the outer coolant jacket to be the same as the total cross section of coolant tubes to maintain the same velocities,^c the coolant tube inner edge-to-edge width $\eta = \sqrt{3}(\omega - 2t_t)$ can be calculated:

$$\eta = \frac{1}{f_p + 1} \left(\sqrt{\frac{2g}{3m}} - 2t_t \right) \text{ where } g = (f_p + 1)(A_i - f_p A_o)\sqrt{3} - 12 m t_t^2 f_p, \quad (2)$$

A_i and A_o are inner and outer areas of the unit fuel cell, $m = 3n(n + 1) + 1$ is the total number of coolant tubes, and $f_p = f_f/\phi$ is the fuel paste volume fraction. Unit cells are separated by twice the jacket thickness.

The two-dimensional steady-state heat equation with temperature-dependent thermal conductivity is a nonlinear Poisson equation, *viz.*

$$\nabla \cdot (\kappa_0 \nabla T) = \kappa_0 \nabla^2 T + \nabla \kappa_0 \cdot \nabla T = \kappa_0 \nabla^2 T + \|\nabla T\|^2 \left. \frac{\partial \kappa_0}{\partial T} \right|_{T=T(x,y)} = Q, \quad (3)$$

where T is temperature ($^{\circ}\text{K}$), Q is thermal power density (W/m^3), and κ_0 is temperature-dependent thermal conductivity ($\text{W}/\text{m}/^{\circ}\text{K}$). This is a proxy for a three-dimensional equation, assuming a 1-mm thick horizontal cross section of a unit cell with negligible vertical temperature gradient and continuous homogeneous Neumann boundary conditions in the vertical direction. Within the cross section, the outer wall and coolant tube boundary conditions are constant Dirichlet conditions, with the coolant temperature taken to be 715°K in studies of an unit cell with dimensions similar to a cell in S-PRISM [7]. This is assumed to be representative of the mid plane of the reaction region.

Equation (3) is nonlinear because κ_0 depends upon temperature T . Sodium thermal conductivity and uranium thermal conductivity have different temperature dependence. The temperature

^cRequiring equal velocities is a crude approximation that does not account for different ‘‘hydraulic diameter’’ and different turbulence in hexagonal tubes and smooth flat rectangular ducts.

dependence of sodium conductivity was taken from [10, p. 181]. A correlation between temperature and uranium thermal conductivity was developed from tables in [11]:

$$\kappa_U = 19.83 - 2.85T + 0.91 \times 10^{-5} T^2 - 0.67 \times 10^{-8} T^3 + 2.78 T^{1.0044} + 1.32 \log(T). \quad (4)$$

Conductivity of a paste of sodium and uranium particles depends upon ϕ and was calculated using

$$\frac{\kappa_p}{\kappa_{Na}} = 1 + 3\beta\phi + 3\beta^2\phi^2 \left(1 + \frac{9\beta}{16(\beta+5)} + \frac{\beta}{4} + \frac{\beta^2}{2^6} + \dots \right) + O(\phi^3), \quad (5)$$

from [12], where $\beta = (\alpha - 1)/(\alpha + 2)$, $\alpha = \kappa_f/\kappa_{Na}$, κ_{Na} = the thermal conductivity of liquid sodium, κ_f = the thermal conductivity of uranium.

The Poisson equation was solved using a finite-element method on a triangular mesh. The usual method to solve nonlinear Poisson equations is to couple a Poisson solver to a Newton iteration. It was found that a fixed-point iteration consisting of alternate Poisson solutions and re-evaluation of κ_0 , $\partial\kappa_0/\partial T$, and $\|\nabla T\|^2$, or κ_0 , $\nabla\kappa_0$, and ∇T , converged very rapidly because κ_0 changes slowly over a small range with respect to temperature. Three iterations were sufficient for 0.1°K agreement, while six iterations were sufficient for 10^{-6} °K agreement.

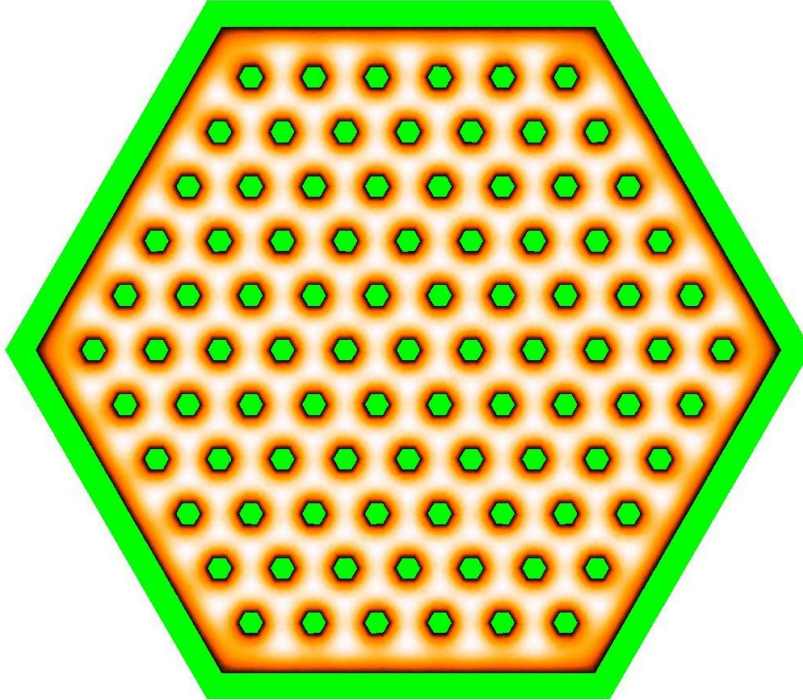
Equation (3) was solved in both the second and third forms. Gradients were computed using an area-weighted average of gradients in each triangle, and by a weighted least-squares fit to a plane passing through each point and its immediate neighbors in the mesh. For the least-squares method, the plane at each vertex of the mesh was constrained to pass through the temperature or conductivity at the vertex of interest, and other points were weighted according to the inverse of their distance from the point of interest. Results using the two methods agreed within five digits. Using the first representation and the least-squares method was substantially faster. A solution of Equation (3) using this method for a unit cell with six tubes on each edge, $f_f = 0.5$, and $\phi = 0.65$ is shown in Figure 2.

Dimensions used for reference and shown in Table I were taken from S-PRISM [7].

TABLE I
S-PRISM Assembly Dimensions

Assembly edge	W	88.19 mm
Fuel slug radius		2.738 mm
fuel slug length		1016 mm
Cladding thickness	t	0.599 mm
Fuel pins per assembly	m	331
Fuel assemblies		131
Fuel fraction within one assembly	f_f	0.283
Power density of fuel	P	902.4 MW/m ³
Assembly outer wall		3.940 mm
Pressure drop	p	60 PSI
Temperature gradient	ΔT	132.9 °K/m

Figure 2: Temperatures



The temperature variation along a line of length s between adjacent coolant tubes is given (approximately) by the solution $T(x) = \frac{Q}{2\kappa_0} x(x-s) + T_c$ of the one-dimensional constant-conductivity steady-state heat equation with the coolant temperature T_c specified at zero and s . An analytic solution is not possible with temperature-dependent conductivity, but a numerical solution produces a similar result.

Calculations were undertaken with

- the number of coolant tubes n along each edge equal to 6, 7, 8, or 9, i.e., $m = 3n(n+1) + 1 = 127, 169, 217, \text{ or } 271$ tubes within a unit fuel cell,
- the fuel volume fraction f_f equal to 0.2, 0.25, 0.3, 0.35, 0.4, 0.45, or 0.5, and
- the fuel volume mixing ratio ϕ in paste equal to 0.65, 0.70, 0.75, 0.80, 0.85, or 0.90.

Fuel power density Q in Equation (3) is ϕ times the power density within solid metal in S-PRISM.

It is clear in Figure 2 that the temperature of cold regions between coolant tubes and the unit cell wall is lower than between coolant tubes. Temperatures in these regions could be increased to nearer the average of other regions by deforming the outer coolant tubes away from the boundary, which would increase the necessary coolant velocity in those tubes to account for their smaller cross sections, or by deforming the outer boundary, which would change the inter-element duct from a rectangle, changing the “hydraulic diameter” and introducing turbulence; the latter change would require to increase the width of the jacket. These configurations were not analyzed.

After the coolant tube size is computed for the specified desired fuel volume fraction, the spacing δ for the tube nearest the corner is determined by iterating the solution of Equation (3) until the average of the maximum temperatures in the hot regions between outermost coolant tubes and the unit cell wall is nearly equal to the average of the maximum temperatures in the next inward region. As shown in Table II for one representative example with nine tubes per edge, $f_f = 0.5$, and $\phi = 0.65$, the average maximum temperatures in radial zones, after solving for δ , are remarkably uniform. This was observed in all solutions, but is not extensively tabulated here for the sake of brevity.

TABLE II
Radial zone average maximum temperatures °K

1	2	3	4	5	6	7	8	9 hot	9 cold
769.333	769.514	769.627	769.521	769.345	769.463	769.457	769.491	769.419	756.417

The coolant flow velocity v_2 within coolant tubes was calculated from Equation (1) using $\rho = 927 \text{ kg/m}^3$, $C_p = 1.256 \text{ kJ/kg/}^\circ\text{K}$ [10, p. 14], and P and ΔT the same as in S-PRISM [7]. The pressure change within coolant tubes was calculated using incompressible flow mass conservation, from which $v_1 = 2 f_c v_2$, and Bernoulli's equation

$$\Delta p = \frac{\rho}{2} (v_2^2 - v_1^2) = \frac{\rho}{2} v_2^2 (1 - 4 f_c^2). \quad (6)$$

Results of the calculations are shown in Tables III through XIV.

TABLE III
 T_{\max} °K with 127 Coolant Tubes

Fuel Volume Mixing Ratio ϕ						
f_f	0.65	0.70	0.75	0.80	0.85	0.90
0.20	781.9	777.9	774.6	773.4	769.5	769.6
0.25	804.6	798.0	793.2	789.1	786.0	784.2
0.30	831.3	822.1	814.0	808.2	803.5	799.8
0.35	866.8	850.8	840.1	830.7	823.9	818.2
0.40	909.2	887.0	869.8	858.2	847.3	840.3
0.45	969.5	933.9	907.9	889.2	876.1	864.4
0.50	1052.6	995.2	956.3	929.2	908.5	894.1

TABLE IV
 T_{\max} °K with 169 Coolant Tubes

Fuel Volume Mixing Ratio ϕ						
f_f	0.65	0.70	0.75	0.80	0.85	0.90
0.20	762.7	760.2	757.7	756.5	754.3	754.0

(cont.)

TABLE IV
 T_{\max} °K with 169 Coolant Tubes (cont.)

Fuel Volume Mixing Ratio ϕ						
f_f	0.65	0.70	0.75	0.80	0.85	0.90
0.25	778.7	774.5	771.2	768.5	765.9	764.4
0.30	798.9	792.0	786.3	782.1	779.5	776.2
0.35	824.1	813.5	805.9	799.1	793.8	789.9
0.40	856.3	839.9	828.3	818.6	811.6	805.5
0.45	900.6	874.6	855.4	842.8	832.7	824.2
0.50	963.1	920.3	891.9	872.1	858.2	846.3

TABLE V
 T_{\max} °K with 217 Coolant Tubes

Fuel Volume Mixing Ratio ϕ						
f_f	0.65	0.70	0.75	0.80	0.85	0.90
0.20	750.8	748.8	747.1	746.6	745.4	743.9
0.25	763.1	759.8	757.2	754.8	753.4	752.2
0.30	778.7	773.0	769.0	765.7	762.9	761.1
0.35	797.6	788.8	783.2	778.7	774.5	771.9
0.40	822.8	809.6	800.5	793.6	787.9	784.1
0.45	856.1	835.5	822.3	812.1	803.6	797.9
0.50	904.7	871.4	850.4	835.1	823.4	814.5

TABLE VI
 T_{\max} °K with 271 Coolant Tubes

Fuel Volume Mixing Ratio ϕ						
f_f	0.65	0.70	0.75	0.80	0.85	0.90
0.20	742.9	741.3	739.9	739.3	737.9	737.6
0.25	752.4	750.1	747.6	746.3	744.9	743.6

(cont.)

TABLE VI
 T_{\max} °K with 271 Coolant Tubes (cont.)

Fuel Volume Mixing Ratio ϕ						
f_f	0.65	0.70	0.75	0.80	0.85	0.90
0.30	764.2	759.9	756.9	754.5	752.4	750.8
0.35	779.3	773.3	767.9	764.3	761.4	758.9
0.40	798.6	788.9	782.0	776.3	772.3	768.6
0.45	825.8	809.7	798.9	790.7	784.9	779.9
0.50	863.8	838.3	821.2	808.9	800.4	793.2

TABLE VII
Coolant Velocity, m/s with 127 Coolant Tubes

Fuel Volume Mixing Ratio ϕ						
f_f	0.65	0.70	0.75	0.80	0.85	0.90
0.20	1.1	1.1	1.1	1.0	1.0	1.0
0.25	1.7	1.6	1.5	1.4	1.4	1.4
0.30	2.4	2.2	2.1	2.0	1.9	1.8
0.35	3.4	3.1	2.8	2.6	2.5	2.3
0.40	5.2	4.4	3.9	3.5	3.3	3.0
0.45	8.3	6.5	5.5	4.8	4.3	4.0
0.50	16.0	10.5	8.1	6.7	5.8	5.2

TABLE VIII
Coolant Velocity, m/s with 169 Coolant Tubes

Fuel Volume Mixing Ratio ϕ						
f_f	0.65	0.70	0.75	0.80	0.85	0.90
0.20	1.2	1.1	1.1	1.1	1.0	1.0
0.25	1.7	1.6	1.5	1.5	1.4	1.4
0.30	2.5	2.3	2.1	2.0	1.9	1.8

(cont.)

TABLE VIII
Coolant Velocity, m/s with 169 Coolant Tubes (cont.)

Fuel Volume Mixing Ratio ϕ						
f_f	0.65	0.70	0.75	0.80	0.85	0.90
0.35	3.6	3.2	2.9	2.7	2.5	2.4
0.40	5.4	4.6	4.0	3.6	3.4	3.1
0.45	8.8	6.8	5.7	5.0	4.5	4.1
0.50	17.3	11.2	8.5	7.0	6.1	5.4

TABLE IX
Coolant Velocity, m/s with 217 Coolant Tubes

Fuel Volume Mixing Ratio ϕ						
f_f	0.65	0.70	0.75	0.80	0.85	0.90
0.20	1.2	1.2	1.1	1.1	1.1	1.0
0.25	1.8	1.7	1.6	1.5	1.5	1.4
0.30	2.5	2.3	2.2	2.1	2.0	1.9
0.35	3.7	3.3	3.0	2.8	2.6	2.5
0.40	5.6	4.7	4.2	3.8	3.5	3.2
0.45	9.3	7.2	5.9	5.2	4.6	4.2
0.50	18.8	11.9	9.0	7.3	6.3	5.6

TABLE X
Coolant Velocity, m/s with 271 Coolant Tubes

Fuel Volume Mixing Ratio ϕ						
f_f	0.65	0.70	0.75	0.80	0.85	0.90
0.20	1.2	1.2	1.1	1.1	1.1	1.1
0.25	1.8	1.7	1.6	1.6	1.5	1.5
0.30	2.6	2.4	2.2	2.1	2.0	1.9
0.35	3.9	3.4	3.1	2.9	2.7	2.6

(cont.)

TABLE X
Coolant Velocity, m/s with 271 Coolant Tubes (cont.)

		Fuel Volume Mixing Ratio ϕ					
f_f		0.65	0.70	0.75	0.80	0.85	0.90
0.40		5.9	4.9	4.3	3.9	3.6	3.3
0.45		9.9	7.5	6.2	5.4	4.8	4.4
0.50		20.6	12.7	9.5	7.7	6.6	5.8

TABLE XI
Pressure Gradient, PSI with 127 Coolant Tubes

		Fuel Volume Mixing Ratio ϕ					
f_f		0.65	0.70	0.75	0.80	0.85	0.90
0.20		0.0	0.0	0.0	0.0	0.0	0.0
0.25		0.1	0.1	0.1	0.1	0.1	0.1
0.30		0.2	0.2	0.2	0.1	0.1	0.1
0.35		0.6	0.4	0.3	0.3	0.2	0.2
0.40		1.4	0.9	0.7	0.6	0.4	0.4
0.45		3.9	2.3	1.5	1.1	0.9	0.7
0.50		15.3	6.4	3.6	2.4	1.7	1.3

TABLE XII
Pressure Gradient, PSI with 169 Coolant Tubes

		Fuel Volume Mixing Ratio ϕ					
f_f		0.65	0.70	0.75	0.80	0.85	0.90
0.20		0.0	0.0	0.0	0.0	0.0	0.0
0.25		0.1	0.1	0.1	0.1	0.1	0.1
0.30		0.3	0.2	0.2	0.1	0.1	0.1
0.35		0.6	0.5	0.4	0.3	0.3	0.2
0.40		1.5	1.0	0.8	0.6	0.5	0.4

(cont.)

TABLE XII
Coolant Velocity, m/s with 169 Coolant Tubes (cont.)

Fuel Volume Mixing Ratio ϕ						
f_f	0.65	0.70	0.75	0.80	0.85	0.90
0.45	4.4	2.5	1.7	1.2	0.9	0.8
0.50	17.9	7.2	4.0	2.6	1.9	1.4

TABLE XIII
Pressure Gradient, PSI with 217 Coolant Tubes

Fuel Volume Mixing Ratio ϕ						
f_f	0.65	0.70	0.75	0.80	0.85	0.90
0.20	0.0	0.0	0.0	0.0	0.0	0.0
0.25	0.1	0.1	0.1	0.1	0.1	0.1
0.30	0.3	0.2	0.2	0.2	0.1	0.1
0.35	0.7	0.5	0.4	0.3	0.3	0.2
0.40	1.7	1.1	0.8	0.7	0.5	0.4
0.45	5.0	2.8	1.9	1.3	1.0	0.8
0.50	21.2	8.2	4.5	2.9	2.1	1.6

TABLE XIV
Pressure Gradient, PSI with 271 Coolant Tubes

Fuel Volume Mixing Ratio ϕ						
f_f	0.65	0.70	0.75	0.80	0.85	0.90
0.20	0.1	0.0	0.0	0.0	0.0	0.0
0.25	0.1	0.1	0.1	0.1	0.1	0.1
0.30	0.3	0.2	0.2	0.2	0.2	0.1
0.35	0.7	0.5	0.4	0.4	0.3	0.3
0.40	1.9	1.3	0.9	0.7	0.6	0.5
0.45	5.6	3.1	2.1	1.5	1.1	0.9

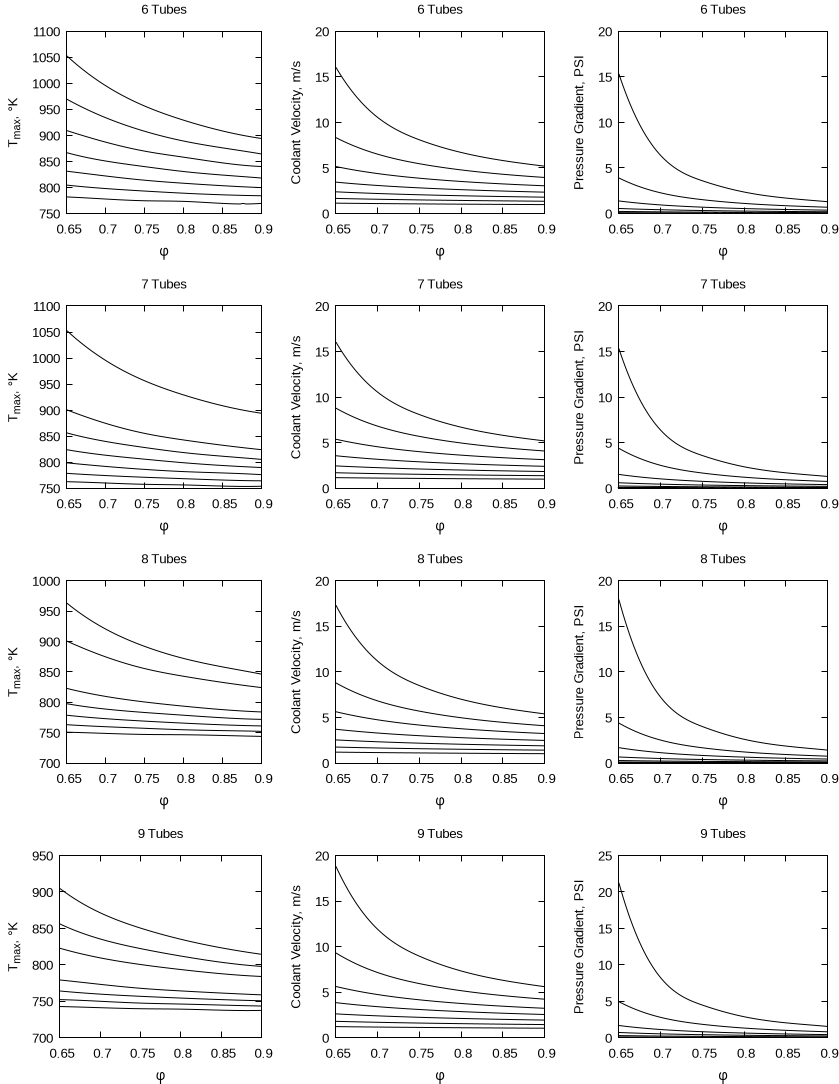
(cont.)

TABLE XIV
Coolant Velocity, m/s with 271 Coolant Tubes (cont.)

Fuel Volume Mixing Ratio ϕ						
f_f	0.65	0.70	0.75	0.80	0.85	0.90
0.50	25.5	9.5	5.1	3.2	2.3	1.7

The results in Tables III through XIV are shown in graphical form in Figures 3 and 4. In Figure 3 the curves, from bottom to top, are for $f_f = 0.20, 0.25, 0.30, 0.35, 0.40, 0.45,$ and 0.50 .

Figure 3: Solutions for $f_f = 0.2 \dots 0.5$



The number of tubes shown in the captions in Figures 3 and 4 are the number of coolant tubes on each edge, not the total number contained, in a unit cell. As the number of tubes increases, temperatures decrease, while coolant velocities and pressure gradients increase. Figure 3 shows that temperatures, coolant velocities, and pressure gradients decrease as ϕ is increased.

In Figure 4 the curves, from top to bottom, are for $\phi = 0.65, 0.70, 0.75, 0.80, 0.85,$ and 0.90 .

Figure 4: Solutions for $\phi = 0.65 \dots 0.90$

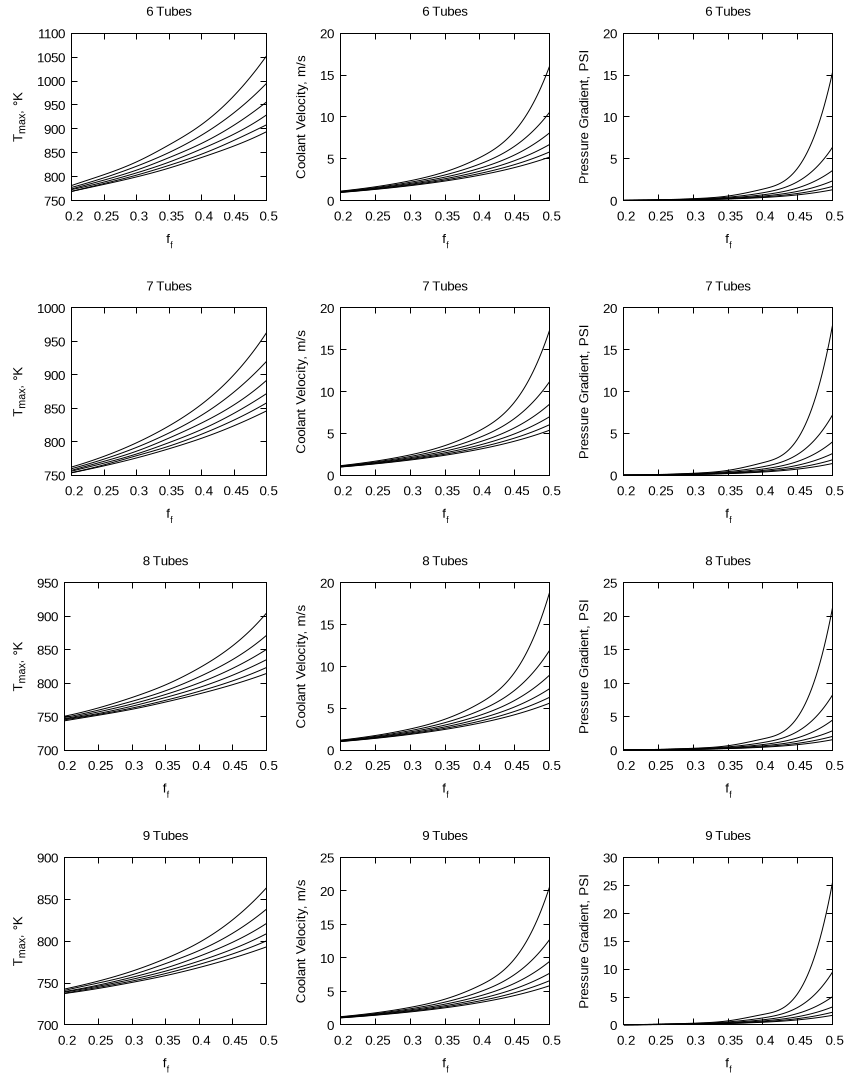


Figure 4 shows that temperatures, coolant velocities, and pressure gradients increase as f_f is increased.

One might expect the coolant flow velocities, and pressure gradients, to be the same for each

value of fuel volume fraction, but those quantities increase slightly as the numbers of tubes increase because the structure fraction increases, and therefore the coolant fraction decreases.

In designing a unit fuel cell for a reactor one would start with criticality analysis, which would depend upon f_f and ϕ ; this was beyond the scope of this study. Within suitable ranges, the number of coolant tubes, fuel volume fraction f_f , fuel volume mixing ratio ϕ within fuel paste, and fissile enrichment (and therefore power density Q) are then chosen to produce desired values of maximum temperature, coolant flow rate, and pressure gradient.

V. IMPLICATIONS FOR POST-IRRADIATION FUEL HANDLING

As Koch explained in [13, p. 3-40], when a fuel assembly was removed from EBR-II for processing, it was necessary to cool it actively until it was disassembled. After disassembly, individual fuel pins were stored less densely, and natural atmospheric convection provided sufficient cooling. Storage for fuel pins awaiting processing was simple.

A unit cell as described here would need active cooling, perhaps outside the core but within the sodium pool in a reactor similar to EBR-II or S-PRISM, until it is opened and emptied for processing.

As explained in [6], some fuel processing proceeds during operation because sodium-soluble fission products migrate into bond sodium, and pyroelectric processing of fuel particles proceeds more quickly because the surface-to-volume ratio is larger than for solid slugs.

VI. IMPLICATIONS FOR CONTROL AND SAFETY

As burnup proceeds, uranium-238 is converted to higher actinides and fissionable actinides are converted to fission product metals having different thermal expansions, and fission product gases that largely escape from particulate fuel, as explained in [6]. Some fission product metals escape from fuel particles into bond sodium, and do not contribute to bulk fuel thermal expansion. Because fuel volume fraction f_f changes very little, and slowly, reactivity swings during burnup are small.

In EBR-II, as temperature increased, fuel assemblies expanded, increasing separation between fuel pins, and the entire core structure expanded, increasing separation between fuel assemblies. This reduced neutron economy, providing a negative relationship of activity to temperature, and contributing to passive safety.

Assume the unit cell is made from HT-9 stainless steel. Relevant thermal expansion coefficients are shown in Table XV.

TABLE XV
Thermal expansion coefficients $\mu\text{m}/\text{m}/^\circ\text{K}$

HT-9 SS	10–13	Sodium	71
Uranium	13.9	Plutonium	46.7
Zirconium	5.7	U-19Pu-10Zr	19.2

With particulate fuel, when bond sodium and dissolved fission products expand due to increased temperature, they flow around fuel, which is 20.7 times more dense than sodium, increasing the height of sodium above fuel. Bond sodium and its dissolved fission products do not contribute to expansion of the bulk fuel mixture.

The bulk fuel mixture thermal expansion coefficient, and its relationship to structural thermal expansion, depend upon the initial fuel alloy and the extent of burnup. If fuel thermal expansion is less than for structure, as temperature increases, the ratio of active height to width decreases. If fuel thermal expansion is greater than for structure, as temperature increases, the ratio of active height to width increases. Which of these regimes holds in a particular reactor, or a particular unit cell, at a particular instant, depends upon the fuel alloy and the extent of burnup.

If structural elements that support fuel cells are similar to EBR-II, as temperature increases, separation between fuel cells would increase, similarly to fuel assembly separation in EBR-II.

Fuel elements as described here could be used in a reactor with mobile paste fuel as described in [8], wherein a separate inherently-safe gravity-connected storage region was proposed.^d

Although FCMI is greatly reduced compared to solid slugs in pins, concerns of FCCI remain. In experiments in EBR-II, it was found that ternary U-10Pu-19Zr fuel greatly re-

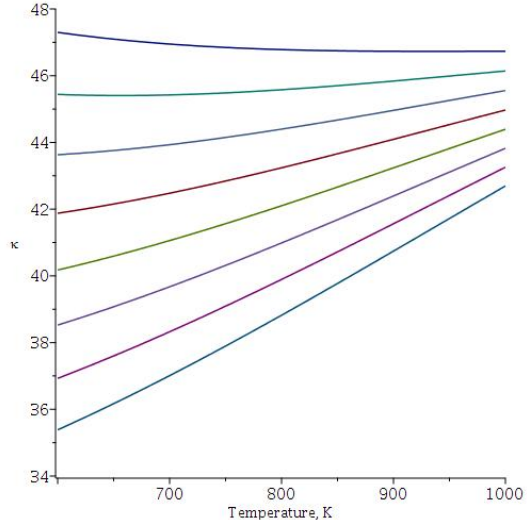


Fig. 6. Fuel Conductivity κ_0 , $\text{W}/\text{m}/^\circ\text{K}$, $\phi = 0.60$ (top) to 0.95 (bottom)

^dEXODYS proposes a similar safety system [14].

duced FCCI. Plutonium-uranium eutectic formation was not found below about 975°K, and eutectic formation at 1075°K was not significant after one hour [1, §6.8]. The maximum temperatures shown in Tables III through XIV occur at maximum distances from coolant tubes or the unit cell boundary. Temperatures are much lower at those boundaries, and therefore eutectic formation is not expected.

Lower stored doppler reactivity is an important safety asset [4]. Stored doppler reactivity would be less than with solid fuel, and much less than with oxide fuel, because the thermal conductivity of a sodium-plus-uranium paste is greater than the conductivity of uranium metal or oxide alone at all operating temperatures and fuel/sodium volume mixing ratios ϕ , as shown in Figure 6. The curves converge at about 1216°K, assuming pressure is sufficiently high that sodium does not boil, because sodium conductivity decreases as temperature increases, while uranium conductivity increases as temperature increases. Higher thermal conductivity also reduces thermal gradients.

Beyond these trivial observations, assessing the effect of thermally-induced changes on passive safety is outwith the scope of this study. Determining whether a reactor fueled using units described here, and incorporating structural elements that increase the space between unit cells as temperature increases, would be passively safe is outwith the scope of this study. Those are questions for which the answers require more knowledge and more tools than the author has.

VII. CONCLUSIONS

The goal of this investigation was limited to determining whether inverting the relationship between fuel and coolant could increase the fuel volume fraction without adversely increasing temperatures, coolant flow rates, and pressure gradients. One can observe that most fuel volume fractions f_f shown in Tables III through XIV are greater than the fuel volume fraction shown for S-PRISM in Table I. The fuel volume fraction depends both upon physical geometry and the volume mixing ratio ϕ in fuel paste, the latter depending upon the distribution of particle sizes [5]. Beyond the benefits of larger f_f cited by Till and Chang [1], larger f_f allows a smaller overall reactor for the same power output.

Most fuel temperatures are well below the 1154°K boiling point of sodium but using only six tubes along each unit fuel cell edge, large values of f_f , and small values of ϕ , might result in

temperatures too large for comfort. Coolant flow rates and pressure gradients are reasonable.

VIII. ACKNOWLEDGEMENTS

The steady-state heat equation was solved using the *Fem2D_Poisson_CG* software for the finite element method, provided by John Burkardt. The region over which the equation was solved was divided into triangles, for use by the finite element method, using the *Triangle* software provided by Jonathan Shewchuk. Several procedures from the Caltech Jet Propulsion Laboratory Math77 library of mathematical software were used [15]. Reference [15], the final NASA technical note about the package, describes version 4.0, but the final version, 6.24, is available from <https://netlib.org/math/>. Figure 2 was prepared by EGGX/ProCALL, the Easy and Gratifying Graphics Library for X11, by Chisato Yamauchi. Other graphics were produced using Gnuplot.

REFERENCES

- [1] C. E. TILL and Y. I. CHANG, *Plentiful Energy: The Story of the Integral Fast Reactor*, CreateSpace (2011) ISBN 978-1466384606.
- [2] G. L. HOFMAN, L. C. WALTERS, and T. H. BAUER, “Metallic Fast Reactor Fuels,” *Progress in Nuclear Energy*, **31**, 1/2, 83 (1997).
- [3] C. E. TILL and Y. I. CHANG, “Progress and Status of the Integral Fast Reactor (IFR) Fuel Cycle Development,” ANL/CP-72650, Argonne National Laboratory (1991).
- [4] Y. I. CHANG, “Technical Rationale for Metal Fuel in Fast Reactors,” *Nuclear Engineering and Technology*, **39**, 3, 161 (2007).
- [5] R. S. FARR and R. D. GROOT, “Close Packing Density of Polydisperse Hard Spheres,” *Journal of Chemical Physics*, **131** (2009); 10.1063/1.3276799.
- [6] W. V. SNYDER, “Finely-Divided Metal as Nuclear Reactor Fuel,” *Nuclear Technology*, **208** (2022); 10.1080/00295450.2021.2024023.
- [7] A. E. DUBBERLEY, “S-PRISM High Burnup Metal-Fuel Core Design,” *Proceedings of ICAPP '03*, American Nuclear Society (2003) Paper number 3142.

- [8] W. V. SNYDER, “Revisiting Mobile Paste Reactor Fuel,” *Nuclear Technology*, **209**, 1840 (2023); 10.1080/00295450.2023.2205551.
- [9] E. E. LEWIS, *Fundamentals of Nuclear Reactor Physics*, Academic Press (2008).
- [10] J. K. FINK and L. LEIBOWITZ, “Thermodynamic and Transport Properties of Sodium Liquid and Vapor,” ANL/RE-95/2, Argonne National Laboratory (1995).
- [11] C. HIN, D. MORGAN, J. YU, and C. PAPESH, “Thermal Conductivity of Metallic Uranium,” NEUP 14-6767, Virginia Tech (Undated).
- [12] D. J. JEFFREY, “Conduction through a random suspension of spheres,” *Proceedings of the Royal Society of London Series A Mathematical and Physical Sciences*, **335**, 1602, 355 (1973); 10.2307/78573.
- [13] L. J. KOCH, *Experimental Breeder Reactor-II: An Integrated Experimental Fast Reactor Nuclear Power Station*, American Nuclear Society (2008) ISBN 978-0-89448-042-1.
- [14] “Exodys Energy,” URL <https://www.exodysenergy.com/copy-of-home>.
- [15] C. L. LAWSON, F. T. KROGH, W. V. SNYDER, C. A. OKEN, F. A. MCCREARY, J. H. LIESKE, J. Z. PERRINE, R. S. COFFIN, and W. J. WAYNE, “Math77, Version 4.0,” *NASA Tech Briefs*, **18**, 3 (1994).

IX. HYDRAULIC DIAMETER

Hydraulic diameter D_h is defined as

$$D_h = \frac{4A_{\text{flow}}}{P_{\text{wetted}}}$$

where A_{flow} is the cross-sectional area of flow, and P_{wetted} is the wetted perimeter.

For a hexagonal channel with edge-to-edge width η

$$D_{h,\text{hex}} = \frac{4\frac{\sqrt{3}}{2}\eta^2}{2\sqrt{3}\eta} = \eta$$

For a thin slab of width W and thickness T , $A_{\text{flow}} = WT$ and $P_{\text{wetted}} = 2(W + T)$. Therefore

$$D_{h,\text{slab}} = \frac{2WT}{W + T}$$

To provide equal heat removal capacities, instead of being equal, the areas of the tubes and jacket should be related according to

$$\frac{A_{\text{tubes}}}{A_{\text{jacket}}} = \frac{D_{h,\text{tubes}}^2}{D_{h,\text{jacket}}^2}$$

Pressure drops in channels are related to velocity by the Darcy-Weisbach relation:

$$\Delta P = f \frac{L}{D_h} \frac{\rho v^2}{2} \quad (7)$$

For low Reynolds numbers, the friction factors are related by the Blasius correlation

$$f = C \text{Re}^{-0.25} = C \left(\frac{\rho v D_h}{\mu} \right)^{-0.25}$$

where μ is dynamic viscosity.

Substituting into the pressure drop Equation (9)

$$\Delta P = C \left(\frac{\rho v D_h}{\mu} \right)^{-0.25} \frac{L}{D_h} \frac{\rho v^2}{2} = \left[C \left(\frac{\rho}{\mu} \right)^{-0.25} \frac{L \rho}{2} \right] v^{1.75} D_h^{-1.25} \quad (8)$$

The pressure drops are necessarily equal. Therefore

$$\frac{v_{\text{jacket}}}{v_{\text{tubes}}} = \left(\frac{D_{h,\text{jacket}}}{D_{h,\text{tubes}}} \right)^{\frac{1.25}{1.75}} = \left(\frac{D_{h,\text{jacket}}}{D_{h,\text{tubes}}} \right)^{\frac{5}{7}}$$

The heat removal rate is proportional to the mass flow rate $q \propto Av$. To equalize heat removal rates we want

$$\frac{q_{\text{jacket}}}{q_{\text{tubes}}} = \frac{A_{\text{jacket}} v_{\text{jacket}}}{A_{\text{tubes}} v_{\text{tubes}}} = \frac{A_{\text{jacket}}}{A_{\text{tubes}}} \left(\frac{D_{h,\text{jacket}}}{D_{h,\text{tubes}}} \right)^{\frac{5}{7}} = 1$$

or

$$\frac{A_{\text{jacket}}}{A_{\text{tubes}}} = \left(\frac{D_{h,\text{jacket}}}{D_{h,\text{tubes}}} \right)^{-\frac{5}{7}}$$

X. HYDRAULIC DIAMETER AND FLOW AREA RELATIONSHIPS

The hydraulic diameter D_h is universally defined as

$$D_h = \frac{4A_{\text{flow}}}{P_{\text{wetted}}}$$

where A_{flow} is the cross-sectional area of the flow domain, and P_{wetted} is the corresponding wetted perimeter.

For an internal regular hexagonal channel with flat-to-flat inner edge width η , the geometric relations yield

$$D_{h,\text{tubes}} = \frac{4 \left(\frac{\sqrt{3}}{2} \eta^2 \right)}{2\sqrt{3}\eta} = \eta$$

For a thin rectangular fluid slab (such as the outer bypass jacket channel) of width W and thickness T , the flow area is $A_{\text{flow}} = WT$ and the wetted perimeter is $P_{\text{wetted}} = 2(W + T)$. Therefore, the exact hydraulic diameter is expressed as

$$D_{h,\text{jacket}} = \frac{2WT}{W + T}$$

Pressure drops in channels are related to velocity by the Darcy-Weisbach relation:

$$\Delta P = f \frac{L}{D_h} \frac{\rho v^2}{2} \quad (9)$$

For fully developed turbulent flow in smooth channels, the friction factors are governed by the Blasius correlation:

$$f = C \text{Re}^{-0.25} = C \left(\frac{\rho v D_h}{\mu} \right)^{-0.25}$$

where μ is the dynamic viscosity of the fluid.

Substituting the friction factor into the pressure drop Equation (9) yields:

$$\Delta P = C \left(\frac{\rho v D_h}{\mu} \right)^{-0.25} \frac{L}{D_h} \frac{\rho v^2}{2} = \left[C \left(\frac{\rho}{\mu} \right)^{-0.25} \frac{L \rho}{2} \right] v^{1.75} D_h^{-1.25} \quad (10)$$

Because the internal tubes and outer jacket channels are connected in parallel between shared inlet and outlet plena, their pressure drops are necessarily equal ($\Delta P_{\text{jacket}} = \Delta P_{\text{tubes}}$). Factoring out the matching constant fluid terms simplifies the real bulk velocity ratio to a function of the hydraulic diameters:

$$\frac{v_{\text{jacket}}}{v_{\text{tubes}}} = \left(\frac{D_{h,\text{jacket}}}{D_{h,\text{tubes}}} \right)^{\frac{1.25}{1.75}} = \left(\frac{D_{h,\text{jacket}}}{D_{h,\text{tubes}}} \right)^{\frac{5}{7}}$$

Assuming the thermal design criteria requires matching bulk fluid energy carrying capacity to the cross-sectional mass flow distribution ($q \propto Av$), equalizing the total heat removal rates ($q_{\text{jacket}} = q_{\text{tubes}}$) requires:

$$\frac{q_{\text{jacket}}}{q_{\text{tubes}}} = \frac{A_{\text{jacket}} v_{\text{jacket}}}{A_{\text{tubes}} v_{\text{tubes}}} = \frac{A_{\text{jacket}}}{A_{\text{tubes}}} \left(\frac{D_{h,\text{jacket}}}{D_{h,\text{tubes}}} \right)^{\frac{5}{7}} = 1$$

This establishes the final self-consistent fluid dynamic area relationship for the geometric design loop:

$$\frac{A_{\text{tubes}}}{A_{\text{jacket}}} = \left(\frac{D_{h,\text{tubes}}}{D_{h,\text{jacket}}} \right)^{-\frac{5}{7}} = \left(\frac{\eta(W + T)}{2WT} \right)^{-\frac{5}{7}}$$